GEOMETRICAL MODELLING OF FRACTURE NETWORKS IN AN ANDESITE-HOSTED GEOTHERMAL RESERVOIR

Warwick Kissling[1], Cécile Massiot[1]

[1]GNS Science, 1 Fairway Drive, Avalon, Lower Hutt 5010.

w.kissling@gns.cri.nz

Keywords: *fractures, networks, borehole imaging, permeability, power law length distributions.*

ABSTRACT

Permeability in geothermal reservoirs hosted in andesitic volcanic rocks is dominantly controlled by faults and fractures, but the connectivity and permeability of these systems are generally poorly constrained. We test the assumption of a truncated power-law distribution for fracture length on fracture networks whose linear density (~0.55 m^{-1}) and orientation (subvertical) matches borehole observations in the Rotokawa Geothermal Field, New Zealand.

Low power law exponents (λ<2.5) yield uniform, fully connected networks on reservoir scales and anisotropic permeability. Higher power law exponents result in low connectivity, and hence low reservoir-scale fracture permeability because of the predominance of short fractures. However, isolated clumps of connected fractures exist with ~50 m scales. For low power law exponents, numerous connected paths of long fractures are found parallel to the main fracture orientation, and produce dominant vertical permeability. By contrast, horizontal connected paths can be found, but are rare and of high tortuosity, permitting very limited horizontal flow. This work provides a baseline for estimating the power law exponent depending on the observed characteristics of a reservoir's permeability.

1. INTRODUCTION

Fracture networks play a dominant role in conducting fluids in low-porosity geothermal reservoirs such as Rotokawa, hosted in andesitic formations (McNamara et al., 2015), or Kawerau, hosted in basement Greywacke (Milicich et al., 2016). Previous studies of fracture systems in the Taupo Volcanic Zone (TVZ) dominantly aimed at characterising fracture distributions and associated permeability in the vicinity of faults, which can act as enhanced conduits or barriers to flow (Rowland et al., 2004). Less attention has been given to pervasive fracture networks located between faults, although they have been observed in boreholes, cuttings (with the presence of veins), drill-cores and borehole image logs (e.g., Milicich et al., 2013; McNamara et al., 2015). While reservoir-scale faults have major impacts on reservoir-scale permeability, as documented at Rotokawa (Hernandez et al., 2015), pervasive fracture networks also contribute to permeability and heat transfer from the fracture system to the matrix, and have significant effects on the mechanical properties of the rock (Kissling et al., 2015).

Fracture length probability distributions can be measured in outcrops, but it is not clear that fracture lengths would necessarily follow the same distribution within geothermal reservoirs. Borehole image logs provide measurements of fracture orientation and densities along the boreholes, but not fracture length. In addition, connectivity away from the borehole cannot be detected (Figure 1; Massiot et al., 2015). Discrete fracture network models allow to test numerically which probability distributions for fracture length are applicable to a particular reservoir (e.g., Davy et al., 2006). These models have provided support for estimating permeability in fractured reservoirs, in a probabilistic sense (Gentier et al., 2011; Barton et al., 2013; Masri et al., 2015). However, this has not yet been attempted for a New Zealand Geothermal Field using "real" field data.

In this paper, we investigate the effect of one statistical distribution of fracture length, a truncated power law, on the connectivity of fracture networks as would occur in fractured reservoir zones located between large faults, where permeability is dominantly controlled by fractures rather than by the matrix. Using simple assumptions, we model 2D fracture networks, and evaluate the potential effects of this distribution on the fracture permeability tensor and on heat transfer between the fracture system and the matrix. We use the example of the Rotokawa Geothermal Field, where fracture densities and orientations have previously been measured in borehole image logs (Massiot et al., 2017a), although the results are generally applicable to any pervasively fractured reservoir.

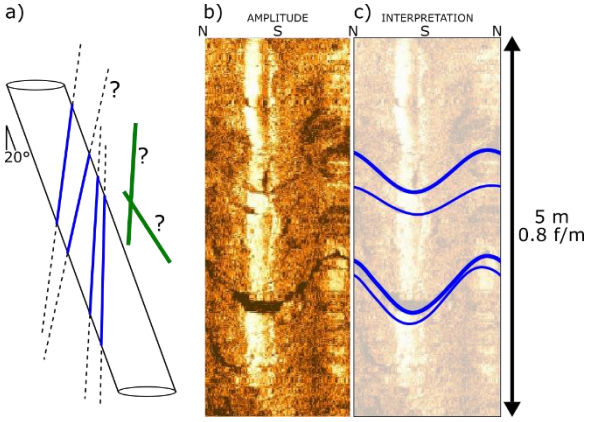

Figure 1: Example of fractures intersecting a borehole. (a) Cartoon depicting steeply-dipping fractures intersecting a 20°-inclined borehole. The length of fractures exterior to the borehole (dashed lines), and presence of nearby fractures (green) is not measurable on image logs. (b) Acoustic amplitude image acquired at Rotokawa, displayed as unrolled with North on the left- and right-hand corners. (c) Image log interpretation with four fractures identified over a 5m interval, yielding a fracture density (0.8 m^{-1}) comparable to the 0.3 - 0.7m^{-1} range observed in three boreholes of the Rotokawa Geothermal Field.

2. MODELLING FRACTURE NETWORKS

2.1 Reservoir Constraints from Borehole Image Logs

The Rotokawa Geothermal Field, located in the Taupo Volcanic Zone, New Zealand, is hosted in an 800-1400m-thick sequence of andesitic formations where porosity is low (typically <10%; Siratovich et al., 2014) and permeability is

dominated by the fracture system (McNamara et al., 2015; McNamara et al., 2016, and references therein). Fracture location, orientation, and morphological characteristics have been analysed directly in the reservoir using three acoustic borehole image logs (Figure 1; McNamara et al., 2015; Massiot et al., 2017a). The linear fracture densities measured along these boreholes (typically deviated 15-25° from the vertical) are 0.4; 0.6 and 0.9 m^{-1}, which reflect spatial variations between the boreholes separated by <500m from each other. Linear fracture densities were measured in intervals where the image log quality does not impact the fracture detection (Massiot et al., 2017b). The average linear density of the >1100 fractures observed along >2km cumulative length of borehole image logs is 0.55 m^{-1}.

There is no proven intersection of these boreholes with the three reservoir-scale faults mapped in the reservoir from stratigraphic offsets, microseismicity and 3D geological modelling (Wallis et al., 2013), although smaller faults are likely to intersect these boreholes based on *in-situ* stress rotations and variations of dip directions observed on the image logs (McNamara et al., 2015).

In this work, we consider that a linear fracture density of ~0.55±0.2 m^{-1} measured along boreholes deviated by ~20° from vertical is representative of areas between the large-scale faults in this reservoir. This is the principle 'observable' to calibrate our models.

Most of the fractures observed in borehole image logs have high (>70°) dip magnitudes (McNamara et al., 2015), and the dip magnitude can be approximated with a normal distribution with mean of 90° (i.e. vertical) and standard deviation of 13°. Several strike orientation populations were observed in the borehole image logs, but only the dominant one is considered here. Corrections for orientation sampling bias, which account for the undersampling of fractures sub-parallel to the boreholes (Terzaghi, 1965; Massiot et al., 2015), show that the linear fracture density, as would be measured along a line orthogonal (in this case horizontal) to the mean fracture dip (vertical), is ~1.7 m^{-1} (Massiot et al., 2017a).

The total fracture porosity (volume of fractures per volume of rock) was estimated to be ~0.05 at image log, core and thin section scales (Massiot et al., 2017a) and is thus a scale independent quantity. In this work, we use this additional criterion to constrain the ratio of fracture width to length in the models. Note that this fracture porosity measurement includes sealed veins which cannot support fluid flow.

2.2 Fracture Network Model Characteristics

We generate fracture networks on a vertical plane through a hypothetical (deviated) wellbore. The model domain size is 350 x 350 m to permit (almost) reservoir-like length scales without having excessive numbers (~10^6 or more) of fractures (Figure 2).

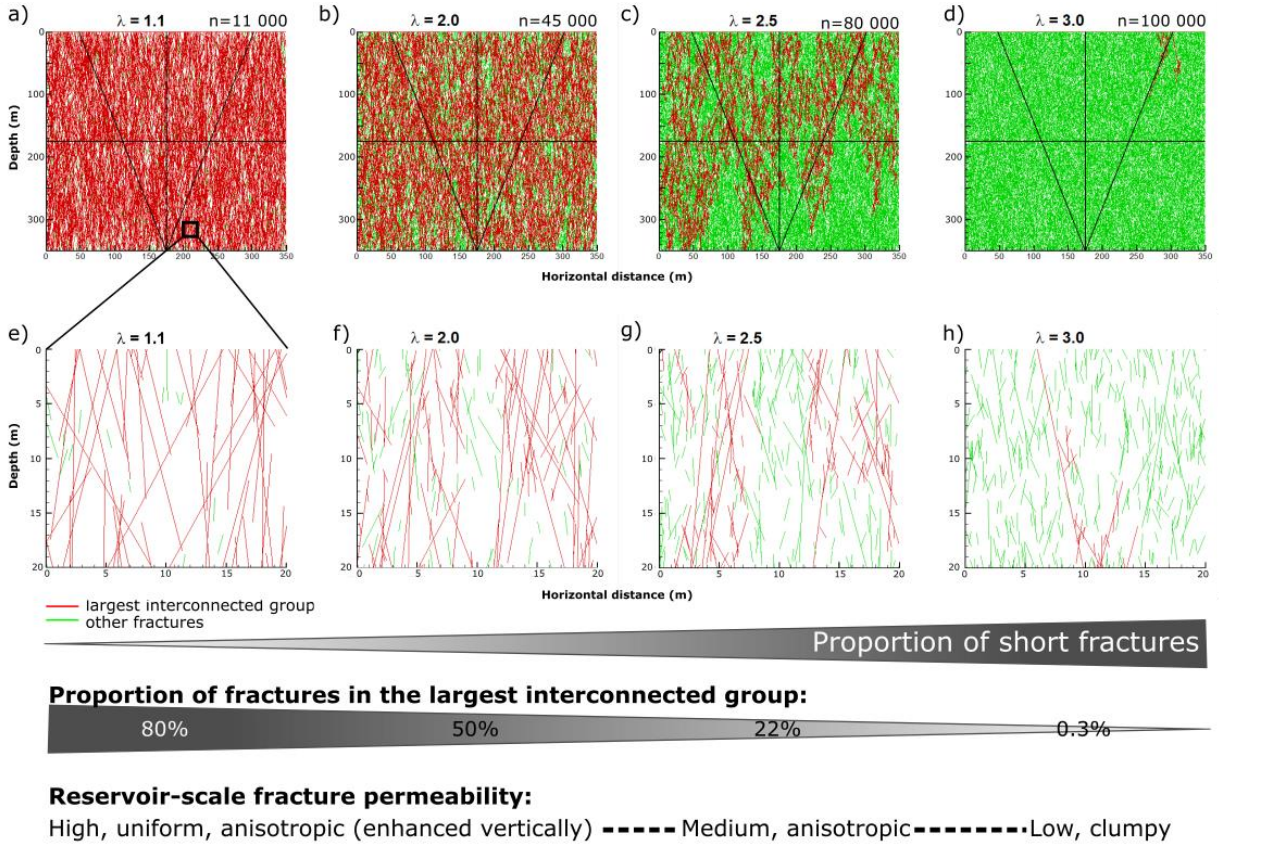

Figure 2. Examples of fracture networks matching the observed linear fracture density of ~0.55 m^{-1} along boreholes deviated 20° from the vertical (black inclined lines). a) λ = 1.1; b) λ = 2; c) λ = 2.5; and d) λ = 3. e-h) 20 x 20 m close-up views which show more clearly the largest connected group (red) and all other (green) fractures not connected to the largest group. *n* is number of fractures. Linear fracture densities along the 'horizontal boreholes' in 2a-d at depth 175 m are consistent with the ~1.7 m^{-1} suggested by orientation sampling bias corrections. The proportion of short fractures increases with λ, and reaches a threshold at λ~2.5 where reservoir-scale permeability switches from being uniform and anisotropic, to clumpy and low.

The process of fracture generation involves generating random variables from suitable probability distributions for the position, length and dip of fractures. The position of the center of each fracture is assumed to follow a uniform distribution in both the horizontal and vertical dimensions. Thus, spatial variations of fracture density are not an input in this study. The probability distribution of fracture dips follows a Normal distribution with the mean and standard deviation as observed in borehole image logs (Section 2.1).

Numerous outcrop measurements indicate that fracture length follows a power law distribution (Bonnet et al., 2001, Davy et al., 2006):

$$N(L) \sim A/L^{\lambda}, \quad (1)$$

where N(L) is the number of fractures of length L, A is a constant and λ is the power law exponent (Figure 3). In this paper we use a truncated power law distribution as recommended by Bonnet et al. (2001). The lower limit of L = 1 m corresponds to the minimum fracture length that would have a good probability of intersecting the borehole. The upper limit, set at L = 100 m, is considered as a lower bound for reservoir-scale faults that are not included in these models and may not follow the same power-law length relationship (Bonnet et al., 2001). This length range covers two orders of magnitude, as recommended for reliable statistical analysis of the networks (Bonnet et al., 2001; Massiot et al., 2017b).

With these limits specified, a constant of proportionality is calculated to convert equation (1) to a probability distribution, and this leaves the power law exponent λ as the sole parameter in our models. We use a common convention that power law exponents are expressed as positive numbers, although the actual values are negative. This is best thought of as using $1/L^{\lambda}$ rather than the exactly equivalent $L^{-\lambda}$.

Most power-law exponents, measured in thin sections, cores, outcrops, aerial photography and seismic scale measurements vary between 1 and 3, with 2 the most common value (Bonnet et al., 2001, and references therein). In this study we use a lower value of λ of 1.1 to avoid the 'logarithmic' behaviour of the probability distribution function that results from integrating the power law with λ=1. Values of λ > 3 give fracture networks which are so poorly connected that they cannot provide a realistic representation of a permeable geothermal reservoir (Figure 2d). The probability density functions of fracture lengths for the five values of λ used in this study highlight the higher proportion of short fractures for high λ (Figure 2).

To assess fracture densities in various dimensions, we use the classic terminology used for discrete fracture networks defined by Dershowitz and Herda (1992): Pij where *i* is the dimension of the sampling domain (i=1 for boreholes, and i=2 for 2D fracture network models) and *j* the dimension of the fracture, being either 0 for fracture counts; 1 for fracture length; and 2 for fracture area. For example, P10 is the fracture density measured along aline, and P20 is the fracture density per unit area.

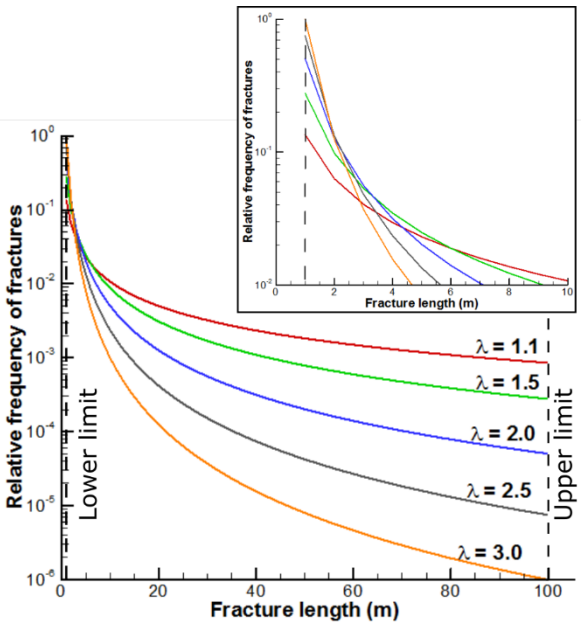

Figure 3: Power law distributions for fracture length (note log-linear scale). The lower and upper limits of fracture length are marked with vertical dashed lines at 1 m and 100 m. This figure shows higher numbers of short fractures for λ = 3.0 compared to other λ's, while conversely, longer fractures are more common for λ= 1.1. Inset: close up of the 0-10m interval highlighting the proportion of short fractures increasing with values of λ.

3. MODELLING RESULTS

3.1 Matching the Observed Linear Fracture Density (P10)

Our first requirement is to match the observed linear fracture density (P10) discussed in section 2.1 with the models. It is not obvious that this can be done for all values of the power law exponent λ, so we first generate fracture networks over the complete range (from 1.1 to 3). Fracture density P10 varies with λ (Table 1), and confirms that we can indeed generate networks with the observed fracture density for any λ. Because there is significant variability between different fracture networks for any particular value of λ, the figures in the table are averages of 20 statistically identical realisations of each network. In the table, all models have calculated fracture densities in the range 0.57 – 0.62 m^{-1}, and are consistent with observation (0.55 m^{-1}) within the typical variability of these figures (see section 2.1). We remark that the number of fractures needed to match the observed linear fracture density increases by an order of magnitude over the range of λ we are considering. Areal fracture densities approach 1 m^{-2} for λ = 3 (the model area is 1.22×10^5 m^2). We also note that the models reproduce the linear fracture density of ~1.7 m^{-1} derived for horizontal wellbores perpendicular to the mean fracture direction when orientation bias corrections are made.

In this paper we have not modelled the flow through the fracture networks, so fracture width is not a relevant quantity. However, the observed (and scale independent) total fracture porosity of 0.05, at thin section, core and image log scales places a loose constraint on the relationship between fracture width and length (Table 1, Massiot et al, 2017a). Fracture width and length have been observed to be correlated (Walmann et al., 1996) and simulations of flow through fracture networks with correlated width to length have been

found to more accurately represent natural systems (Klimczak et al., 2010). Gudmundsson (2000) estimated a ratio of fracture width to length of 1/400, based on outcrop measurements of mineral-filled veins in basalts. For the networks presented here a constant ratio of fracture width to length of 1/100 implies a total fracture porosity of ~1 for some of the range of λ and is thus too high. A ratio of 1/1000 gives more reasonable total fracture porosities between approximatively 0.01 and 0.10. This fracture porosity is consistent with that estimated at Rotokawa (0.05), though it is slightly higher than those found on an outcropping young andesite lava flow in nearby Mt Ruapehu (0.005; Massiot et al., 2017c). A ratio of 1/1000 also provides fracture widths ranging between 1mm and 10cm for our assumed range of fracture length, which is consistent with image log and core measurements (Figure 1; McNamara et al., 2015; Massiot et al., 2017a). This fracture width, which includes open fractures and sealed veins indiscriminately, greatly exceeds the hydraulic aperture found to be <1 or even <0.01 mm in other geothermal fields (Barton et al., 2013; Masri et al., 2015).

Power law exponent (λ)	Number of fractures	Fracture density P10 (m^{-1})	Fracture porosity P22; P33
Rotokawa Observed		0.55* [0.4-0.9]*	0.05*
1.1	11 000	0.58	0.080
1.5	22 000	0.62	0.065
2.0	45 000	0.60	0.037
2.5	80 000	0.62	0.018
3.0	100 000	0.57	0.008

Table 1. Summary of a) fracture numbers needed to match the measured linear fracture density, b) the calculated fracture densities along theoretical 20°-inclined boreholes and c) the total fracture porosity assuming a width/length ratio of 1/1000 for all fractures (see discussion in section 3.1). The fracture density and porosity represent the averages of 20 statistical realisations of each fracture network. In the first row, measurements made in borehole image logs in the Rotokawa reservoir are indicated by *. In the final column, the fracture porosity of 0.05 is evaluated in 3D (P33), while the models provide 2D estimates of fracture porosity (P22).

Figure 4 shows fracture densities P20, P21 and P22 for the networks listed in Table 1. Again, the curves represent the average of 20 realisations for each λ. The number of fractures per unit area (P20) increases with λ, as expected by the higher proportion of short fractures which have a low probability of intersecting the boreholes (Gentier et al., 2011). The opposing effects of increasing the number of fractures and decreasing their length, which occurs with increasing λ, compensate each other to provide a nearly constant fracture length per unit area (P21). However, as the proportion of short, and hence narrow, fractures increases with λ, the fracture area per unit area in the model (P22) decreases.

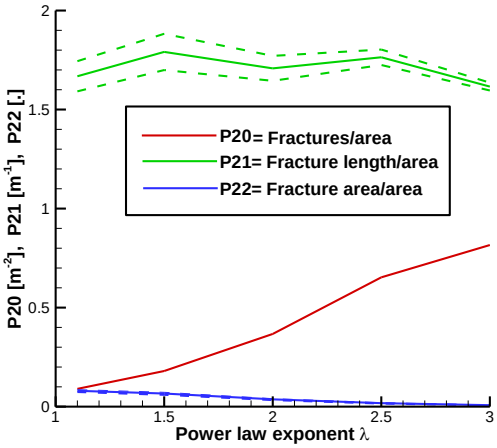

Figure 4. Fracture network density as a function of the power law exponent λ (average of 20 statistical realisations of each fracture network). The dashed lines show the three-standard deviation limits, based on 20 realisations. Because the number of fractures is the same in each realisation for each value of λ, the standard deviation of the areal fracture density P20 is zero.

3.2 Clustering and Connectivity of Fracture Networks

Although all of the networks reproduce the observed linear fracture density along the theoretical deviated boreholes, the topology of fracture networks varies significantly with power law exponents λ.

An important basic feature of the networks is the extent of their connectivity. The red fractures in Figures 2a-d show the largest connected group of fractures in each network. For example, in Figure 2a, with λ=1.1, nearly all fractures (80%) are connected in a single group which extends across the whole model (and is therefore assumed to extend to reservoir scales). In contrast, for λ=3 (Figure 2d), the largest group in the network contains only 0.3% of the fractures, is at most ~100 m in extent, and results in a poorly connected model.

In Figure 2, the green fractures are all those which are not connected to the largest (red) group. The nature of these 'unconnected' fractures is more obvious in the close-ups shown in Figures 2 e-h. They tend to be shorter, and sparsely distributed for λ=1.1, but dominate the fracture density at λ=3.0. For all values of λ, the longest connected path of these 'unconnected' fractures is only a few 10s of metres so they are unable to provide any reservoir-scale permeability.

Another, related, property of the fracture networks is the tendency of fractures to form interconnected groups (clusters) which are hydraulically isolated from the rest of the model domain. This has clear implications for the extent of connected permeability of the fracture networks. Figure 5a shows the number of fractures in the largest such group in each network (black curve). This first increases with λ, reaches a broad maximum at λ ~2, and decreases essentially to zero at λ~3. The same data are reproduced in Figure 5b, but this time plotted (with a vertical log scale) relative to the number of fractures in each network. This confirms that, for λ=1.1, the largest group comprises >80% of all fractures, but this proportion reduces as λ increases, with most of the decline occurring for λ > ~2.5.

In addition, λ ~2.5 marks the transition between large fully connected groups of fractures at low λ and 'clumpy' smaller ones at high λ (Figure 2c). For λ=2.5, the fracture network is fully connected across the model, which would allow for pervasive fluid flow at reservoir scales, but the network contains large areas which are dominated by unconnected fractures. This is even more striking for λ=3, where the areal fracture density P20 is much higher, but is associated with poorer overall connectivity.

An important consequence of the large proportion of unconnected fractures for λ=3.0 is that, although the location of the fractures is uniformly distributed, the fracture network is naturally compartmentalised. This is shown in Figure 6, which shows the ten largest groups of fractures in this network. These are all of roughly the same size, with small numbers of fractures (~200±100), small areas (~100 m^2) and with a linear extent of ~50 m which is insufficient to allow fluid flow at reservoir scales of ~ 1 km or more.

In addition, the number of fracture intersections is approximately independent of the power law exponent (Figure 5a) and seems to be related to the 'fracture intensity' P21 (Figure 4). So, even a high connectivity, as would be measured in outcrops by the numbers of intersections of each fracture, would not necessarily guarantee reservoir-scale connectivity.

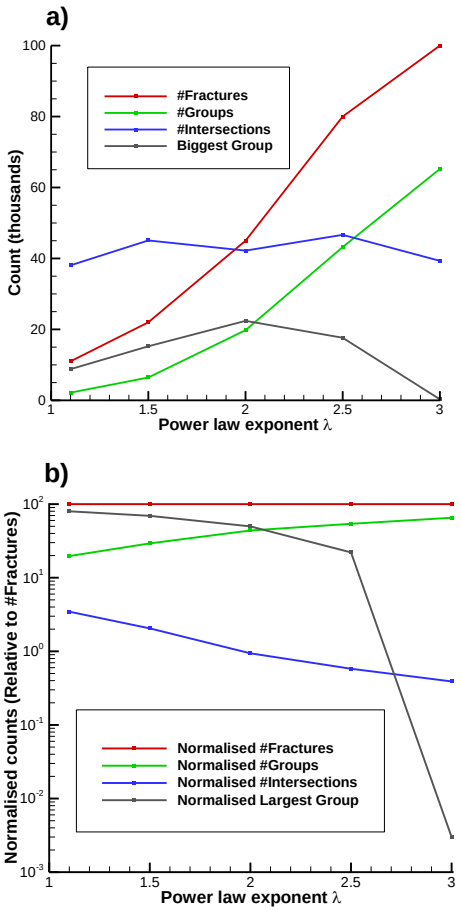

Figure 5. Fracture network clustering as a function of the power law exponent λ, displaying the total number of fractures, the number of interconnected groups, the number of fracture intersections, and the number of fractures in the largest group. a) Linear vertical scale for actual counts and b) Logarithmic vertical scale with all counts normalised by the number of fractures.

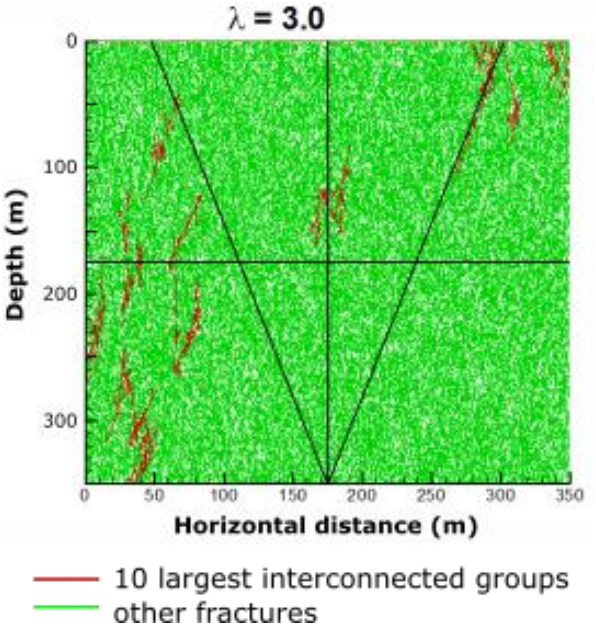

Figure 6. Example of fracture network matching the observed linear fracture density of ~0.55 m^{-1} for λ = 3 showing the ten largest groups, clustered and scattered through the model.

4. DISCUSSION

The geometric models of fracture systems presented here can be applied to fractured reservoirs where permeability is dominantly controlled by the fracture system, and with low matrix permeability. While based on borehole data from the andesite-hosted Rotokawa reservoir, the results are generic and are also relevant to other fractured reservoirs such as the greywacke-hosted Kawerau geothermal system.

4.1 Implications of the λ Value for Upscaling to Reservoir-scale Models

Detailed modelling of the flows through fracture networks is very difficult because of the range of length scales involved, which would require unprecedented numbers of model elements (for the geothermal industry in New Zealand) and the need to simulate heat and fluid transport in large numbers of 'statistically identical' fracture networks.

At a fixed linear fracture density along boreholes, the power-law length coefficient λ has a major influence on the connectivity, and hence reservoir-scale permeability. For λ<2.5 where longer fractures dominate, fracture networks are well connected at 350m scales and thus highly likely to be also fully connected at reservoir scales. The permeability would be uniform (i.e. the same within all parts of the reservoir) but anisotropic, with flow preferentially aligned along the dominant fracture orientation (i.e. vertical in this case). Thus, a single anisotropic permeability tensor would characterise well the contribution of fractures to the permeability. On the contrary, for λ>2.5, the permeability is clumpy, which prevents the use of a single fracture permeability tensor. The fracture permeability may even be

considered to reach a minimum at λ~3 because of the lack of connectivity, in spite of there being many more fractures compared to lower λ models.

Bour and Davy (1997), have carried out an extensive study of the geometrical properties of fracture networks when the fracture length is described by a power law distribution. They concentrate on fracture networks of constant fracture density (P20), and allow fractures longer than the system size on all scales. They derive scaling properties of networks near the 'percolation threshold', where the fracture network becomes fully connected.

In contrast, in this paper we consider a fixed-scale model, appropriate to an andesite lava flow, and use a doubly-truncated power law for fracture length where the maximum length is somewhat less than the system size. Our fracture densities are chosen, for each power law exponent, to match measurements made in > 2 km of borehole imaging from three wells in the Rotokawa geothermal field. We identify a critical power law exponent of ~2.5 where the fracture network becomes fully connected, which corresponds to the 'percolation threshold' of Bour and Davy.

4.2 Fracture Networks Permeability

The nature of the connected fracture paths on a reservoir scale (here 350 m) is a useful indicator of what the permeability of the reservoir might be. Figure 7 shows examples of two such paths extracted from the λ=1.1 fracture network. These paths cross the 'reservoir' in directions which are parallel to (red) and orthogonal (blue) to the average dip of the fractures (i.e. exactly vertical). To construct these paths, the first member of each path is the longest fracture which crosses each of the 'x' and 'y' axes, and which is nearest to the middle (175 m) of its respective axis, to allow for possible large 'sideways' excursions. Subsequent fractures in each path are selected recursively by choosing the fracture which a) is connected to the last member of that path and b) extends the most distance in the desired direction of path propagation. These paths, which are pre-selected by the algorithm to contain long (and therefore wide) fractures, are more likely to be permeable and act as conduits for fluid flow.

The two paths shown in Figure 7 have very different topologies. For the 'red' path, aligned with the mean direction of dip, only seven fractures are required to span the model and the standard deviation of their dip directions is ~12°, consistent with that of the overall population of fractures. In contrast, for the 'blue' path, orthogonal to the average angle of dip, 23 fractures are required to cross the model, and these are preferentially highly inclined to the mean dip direction.

Pathways parallel to the mean fracture direction are rather easier to find by the method outlined above than those orthogonal to it. This suggests that, while connectivity (and therefore permeability) in the parallel pathway will be dominated by the longer (and wider) fractures, the connectivity in the orthogonal direction due to the longest fractures is likely to be much lower. The contribution of shorter fractures to the connectivity, which our simple search technique does not explore, is not known but will likely be a strong function of λ, with the possibility of there being multiple paths with much greater tortuosity than the examples shown in Figure 7. Though greater in number (particularly for high λ) the effect of short fractures is partially offset by their inability to provide connectivity over large distances.

The two connected paths in Figure 7 have very different tortuosities, and the permeability of each will depend on the number of fracture segments (or equivalently the number of intersections) and the total fracture length within each path. For these paths, these numbers are both a factor of ~3-4 larger for the orthogonal path than they are for the parallel path. When considering the flows in real fractures carrying mineralised fluid, rates of solute deposition will likely be enhanced at fracture intersections and on fracture walls through 'gradient reactions' (Phillips, 1991). Thus, flow through the 'blue' high tortuosity path would likely be impeded (or even blocked) by mineral deposition more than in the 'red' path, particularly at conditions typical of geothermal reservoirs where minerals can precipitate within a few weeks (Sonney and Mountain,2013).

So, permeability is likely to be higher in the direction aligned with the dominant fracture orientation, and also be maintained for a longer period of time. However, although they are difficult to construct, flow paths orthogonal to the main fracture orientation may occur, accompanied by longer transport time, and higher probability of being blocked by mineral precipitation.

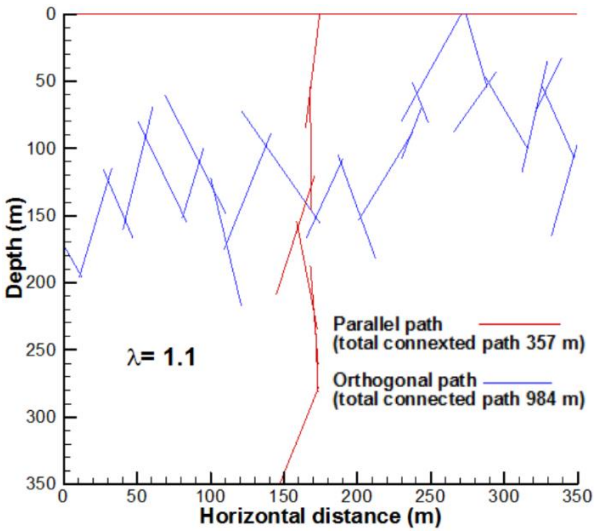

Figure 7. Examples of fully connected paths crossing the model domain in the direction of the mean dip (red) and orthogonal to the mean dip direction (blue), for the λ = 1.1 fracture network.

4.3 Heat Transfer

The ability of the fracture system to permit the transport of hot (or cold) fluid is of great importance to the geothermal industry. While the rigorous calculation of heat and fluid flows in discrete fracture networks of the type presented in this paper is difficult and is the subject of many studies (e.g., Masri et al., 2015), this has not so far been applied to any New Zealand geothermal system. Simple considerations of heat transfer through the fracture system can be quite informative.

The total connected fracture length of the largest groups (green curve, Figure 4, multiplied by the model area) allows to estimate a representative length scale Δ for a 'block' of

matrix material. This is done by equating the total fracture length to that of an idealised fracture network consisting of two orthogonal sets of N parallel fractures with total length 2NX, where X is the largest dimension of the model (here 350 m) and $N = X/\Delta$. For the models here we find N~250-300 (and independent of λ), and therefore $\Delta \sim 1$m.

Considering temperature conduction into the (essentially impermeable) matrix we have $\Delta^2/(4DT) \sim 1$, where T is the representative timescale for heat conduction and D is the thermal diffusion coefficient. Typically, $D \sim 10^{-6}$ m^2s^{-1}, and so we find T is therefore ~ 3 days. This is the response time for a well-connected fracture network (all models with $\lambda \leq 2$), subject to 'instantaneous' filling of the fracture network with fluid of some different temperature ΔT from the matrix – for example caused by injection of cool reinjected brine. Once allowed to equilibrate, the temperature of the combined fracture/matrix block will be $P22.\Delta T$, where P22 is the fracture porosity of ~0.05 (assuming that all fractures are fully open to fluid flow).

4.4 Future Work

The simple models presented in this work allow to test the influence of the fracture length power-law exponent on the topology and connectivity of the reservoir. Although the power-law distribution for fracture length is commonly used (Bonnet et al., 2001), it is unclear that it is always applicable. Massiot et al. (2017a) suggested that the layering caused by the sequence of volcanic rocks in the Rotokawa reservoir influences the location of fractures, so it is possible that this layering may also affect the fracture length, with possible confinement of fracture growth at layer interfaces such as in sedimentary layers (Schopfer et al., 2011, Ferrill 2017). We thus recommend to test the relevance of other statistical length distributions (log-normal, exponential). Constraints on the form of the probability distribution and parameters describing fracture length can arise from a combination of (1) outcrop measurements in exposures analogue to the lithology and tectonics of the reservoir, (2) a qualitative evaluation of the uniformity of the permeability tensor ("uniform" or "clumpy"), and (3) matching of equivalent permeability tensors to reservoir data.

Additional fracture populations with different orientations to the dominant fracture population can significantly increase the connectivity and permeability of fracture networks (Kissling et al., 2015) and are documented at Rotokawa (McNamara et al., 2015), other geothermal fields (McNamara et al., 2016) and in active fault mapping (Villamor et al., 2017). Including these subordinate orientations in the fracture networks would be particularly important in evaluating the connectivity of fracture networks in 3D.

Generic connected pathways through the fracture networks need to be further developed. This will allow better understanding of the role of shorter fractures in providing connectivity, and also the contribution made by the multiple high-tortuosity paths which are likely to occur.

Finally, the models represent the fracture system between faults, without any consideration of spatial variation of fracture location. Increased fracture densities near active faults, documented in outcrops (Mitchell et al., 2009) and in reservoirs (Johri et al., 2014), typically call for spatial correlation of fractures due to faulting. While this increased fracture density near faults has not yet been demonstrated at reservoir conditions in any TVZ geothermal system, it remains an important concept to evaluate.

5. CONCLUSION

We have generated synthetic 2D fracture networks for a single population of sub-vertical fractures, for a family of truncated power law distributions for fracture length. Generated fracture densities are consistent with linear fracture densities measured in acoustic borehole image logs. In all cases connectivity is dominated by longer fractures. This implies that for models with high power law exponent λ, where there are more short fractures, the connectivity of the fracture networks on reservoir scales is reduced.

For power law exponents λ<~2.5, the generated fracture networks are connected on kilometre scales and so are consistent with there being widespread permeability in the reservoir. For modelling purposes, fracture networks for this range of λ can be considered as having uniform and anisotropic permeability. For the highest power law exponent (λ=3), there is little connectivity on scales >~100 m. Networks with such high λ will therefore have poor permeability on reservoir scales and are probably ruled out for New Zealand geothermal systems for this reason. Constraining the form of the probability distribution and parameters describing the fracture lengths relevant to a particular reservoir can be guided by the models presented in this paper.

The fracture porosity, observed to be ~0.05 at all length scales, places a loose constraint on the relationship between fracture width and length. For the data used here, a constant width to length ratio of 1/1000 naturally implies that the fracture porosity is consistent with the observed magnitude. Establishing the relationship between geometric and hydraulic fracture apertures in TVZ geothermal lithologies remains an important and as yet untackled research question.

ACKNOWLEDGEMENTS

This Research is supported by the Government of New Zealand through the GNS Science Supermodels programme. We thank Mercury New Zealand for access to borehole data.

REFERENCES

Barton, C. A., Moos, D., Hartley, L., Baxter, S., Foulquier, L., Holl, H., & Hogarth, R. (2013). Geomechanically coupled simulation of flow in fractured reservoirs. Proceedings of the 38th Workshop on Geothermal Engineering, Stanford.

Bonnet, E., Bour, O., Odling, N. E., Davy, P., Main, I., Cowie, P. A., & Berkowitz, B. (2001). Scaling of fracture systems in geological media. *Reviews of Geophysics*, 39(3), 347–383. doi: 10.1029/1999RG000074

Bour, O., & Davy, P. (1997). Connectivity of random fault networks following a power law fault length distribution. *Water Resources*, *33*(7), 1567–1583. doi: 10.1029/96WR00433

Davy, P., Bour, O., de Dreuzy, J.-R., & Darcel, C. (2006). Flow in multiscale fractal fracture networks. Fractal

Analysis for Natural Hazards, 261(May 2007), 31–45. Doi: 10.1144/GSL.SP.2006.261.01.03

Dershowitz, W. S., and A. H. Herda (1992), Interpretation of fracture spacing and intensity, *33th U.S. Symposium on Rock Mechanics (USRMS)*.

Ferrill, D. A., Morris, A. P., McGinnis, R. N., Smart, K. J., Wigginton, S. S., & Hill, N. J. (2017). Mechanical stratigraphy and normal faulting. *Journal of Structural Geology*, 94, 275–302. Doi: 10.1016/j.jsg.2016.11.010

Gentier, S., Rachez, X., Ngoc, T., Dung, T., Peter-Borie, M., & Souque, C. (2010). 3D flow modelling of the medium-term circulation test performed in the deep geothermal site of Soultz-sous-Forêts (France). World Geothermal Congress.

Gudmundsson, A. (2000). Fracture dimensions, displacements and fluid transport. *Journal of Structural Geology*, 22(9), 1221–1231. doi: 10.1016/S0191-8141(00)00052-3

Hernandez, D., Clearwater, J., Burnell, J., Franz, P., Azwar, L., & Marsh, A. (2015). Update on the Modeling of the Rotokawa Geothermal System: 2010-–2014. Proceedings of the World Geothermal Congress.

Johri, M., Dunham, E. M., Zoback, M. D., & Fang, Z. (2014). Predicting fault damage zones by modeling dynamic rupture propagation and comparison with field observations. *Journal of Geophysical Research: Solid Earth*, 119(2), 1251–1272.

Kissling, W. M., Ellis, S. E., McNamara, D. D., & Massiot, C. (2015). Modelling Fluid Flow Through Fractured Rock: Examples Using TVZ Geothermal Reservoirs. Proceedings 37th New Zealand Geothermal Workshop.

Klimczak, C., Schultz, R. A., Parashar, R., & Reeves, D. M. (2010). Cubic law with aperture-length correlation: implications for network scale fluid flow. *Hydrogeology Journal*, 18(4), 851–862. Doi: .1007/s10040-009-0572-6

Masri, A., Barton, C. A., Hartley, L., & Ramadhan, Y. (2015). Structural Permeability Assessment Using Geological Structural Model Integrated with 3D Geomechanical Study and Discrete Fracture Network Model in Wayang Windu Geothermal. Proceedings of the 40th Workshop on Geothermal Reservoir Engineering, Stanford.

Massiot, C.; Nicol, A.; McNamara, D.D.; Townend, J. (2017a). Evidence for tectonic, lithologic and thermal controls on fracture system geometries in an andesitic high-temperature geothermal field. *Journal of Geophysical Research*, 122(8), 6853-6874. Doi: 10.1002/2017JB014121.

Massiot, C.; Townend, J.; Nicol, A.; McNamara, D.D. (2017b). Statistical methods of fracture characterisation using acoustic borehole televiewer log interpretation. *Journal of Geophysical Research*, 122(8), 6836-6852. Doi: 10.1002/2017JB014115.

Massiot, C., Nicol, A., Townend, J., Mcnamara, D. D., Garcia-sellés, D., Conway, C. E., & Archibald, G. (2017c). Quantitative geometric description of fracture systems in an andesite lava flow using terrestrial laser scanner data. *Journal of Volcanology and Geothermal Research*, 341, 315-331. Doi: 10.1016/j.jvolgeores.2017.05.036

Massiot, C., McNamara, D. D., & Lewis, B. (2015). Processing and analysis of high temperature geothermal acoustic borehole image logs in the Taupo Volcanic Zone, New Zealand. *Geothermics*, 53, 190–201. doi: 10.1016/j.geothermics.2014.05.010

McNamara, D. D., Massiot, C., Lewis, B., & Wallis, I. C. (2015). Heterogeneity of structure and stress in the Rotokawa Geothermal Field, New Zealand. *Journal of Geophysical Research: Solid Earth*, 120(2). Doi: 10.1002/2014JB011480.

McNamara, D. D., Sewell, S. M., Buscarlet, E., & Wallis, I. C. (2016). A review of the Rotokawa Geothermal Field, New Zealand. *Geothermics*, 59(B), 281–293. doi: 10.1016/j.geothermics.2015.07.007

Milicich, S. D., Wilson, C. J. N., Bignall, G., Pezaro, B., & Bardsley, C. (2013). Reconstructing the geological and structural history of an active geothermal field: A case study from New Zealand. *Journal of Volcanology and Geothermal Research*, 262, 7–24. Doi: 10.1016/j.jvolgeores.2013.06.004

Milicich, S. D., Clark, J. P., Wong, C., & Askari, M. (2016). A review of the Kawerau Geothermal Field, New Zealand. *Geothermics*, 59, 252–265. Doi: 10.1016/j.geothermics.2015.06.012

Mitchell, T. M., & Faulkner, D. R. (2009). The nature and origin of off-fault damage surrounding strike-slip fault zones with a wide range of displacements: A field study from the Atacama fault system, northern Chile. *Journal of Structural Geology*, 31(8), 802–816. doi: 10.1016/j.jsg.2009.05.002

Sonney, R., & Mountain, B. W. (2013). Experimental simulation of greywacke-fluid interaction under geothermal conditions. *Geothermics*, 47, 27–39. Doi: 10.1016/j.geothermics.2012.11.003

Rowland, J. V., & Sibson, R. H. (2004). Structural controls on hydrothermal flow in a segmented rift system, Taupo Volcanic Zone, New Zealand. *Geofluids*, 4(4), 259–283. doi: 10.1111/j.1468-8123.2004.00091.x

Phillips, O. M., (1991). Flow and Reactions in Permeable Rocks. Cambridge University Press. 285 pp.

Schöpfer, M. P. J., Arslan, A., Walsh, J. J., & Childs, C. (2011). Reconciliation of contrasting theories for fracture spacing in layered rocks. *Journal of Structural Geology*, 33(4), 551–565. Doi: 10.1016/j.jsg.2011.01.008

Siratovich,P.A., Heap M. J., Villenueve M.C., Cole J. W., and Reuschlé T. (2014). Physical property relationships of the Rotokawa Andesite, a significant geothermal

reservoir rock in the Taupo Volcanic Zone, New Zealand, *Geothermal Energy*, 2,1–31. doi:10.1186/ s40517-014-0010-4.

Terzaghi, R. D. (1965). Sources of error in joint surveys. *Geotechnique*, 15(3), 287–304. doi: 10.1680/geot.1965.15.3.287

Villamor, P., Nicol, A., Rowland, J.R., Seebeck, H., Townsend, D., McNamara, D.D., Milicich, S., Massiot, C., Ries, W. (2017). Tectonic structure and permeability in the Taupo Rift: new insights from analysis of LiDAR derived DEMs. *Proceedings* 39th *New Zealand Geothermal Workshop 2017, Rotorua*.

Wallis, I. C., Bardsley, C., Powell, T., Rowland, J. V., & Brien, J. M. O. (2013). A structural model for the Rotokawa Geothermal Field, New Zealand. *Proceedings* 35th *New Zealand Geothermal Workshop 2013*.

Walmann, T., Malthe-Sørenssen, A., Feder, J., Jøssang, T., Meakin, P., & Hardy H. H. (1996). Scaling Relations for the Lengths and Widths of Fractures. *Phys. Rev. Lett*. 77 (27-30). doi: 10.1103/PhysRevLett.77.5393